Available online at www.sciencedirect.com
ScienceDirect
Trans. Nonferrous Met. Soc. China 30(2020) 571−581
Transactions of Nonferrous Metals Society of China
www.tnmsc.cn

Role of Ca in hot compression behavior and microstructural stability of AlMg5 alloy during homogenization

Bong Huang KIM[1,2], Majid SEYED SALEHI[3], Ashkan NOURI[4], Mohammad Sadegh MOHEBI[5], Seong Ho HA[1], Young Ok YOON[1], Hyun Kyu LIM[1], Shae K. KIM[1], B. Ghasem EISAABADI[4]

1. Korea Institute of Industrial Technology, 156 Gaetbeol-ro, Yeonsu-gu, Incheon 21999, Korea;
2. Department of Materials Science & Engineering, Yonsei University, 262 Seongsan-ro, Seodaemun-gu, Seoul 120-749, Korea;
3. Faculty of Materials Science and Engineering, K. N. Toosi University of Technology, Tehran, Iran;
4. Department of Materials Science and Engineering, Faculty of Engineering, Arak University, Arak 38138-5-3945, Iran;
5. Department of Mechanical Engineering, Qom University of Technology, Qom, Iran

Received 24 May 2019; accepted 24 December 2019

Abstract: Effects of a minor Ca addition on microstructural stability and dynamic restoration behavior of AlMg5 during hot deformation were investigated. They were studied using scanning electron microscopy (SEM), differential scanning calorimetry (DSC), electron backscatter diffraction (EBSD) analyses and transmission electron microscopy (TEM). JMatPro package was used for simulation of the solidification path of the alloys. The results show that the addition of Ca does not affect the microstructure and hot compression behavior of the as-cast samples. However, it prevents the drastic grain growth during homogenization. It is found that coarse grains of Ca-free alloy promote the dynamic recovery and slow down the dynamic recrystallization during hot compression. Also, the particle stimulated nucleation is suggested as the main nucleation mechanism of new recrystallized grains for hot compressed Ca-free alloy. On the other hand, the microstructure of the hot compressed Ca-added alloy is greatly affected by the presence of Al_4Ca intermetallics. The formation of Al_4Ca phase is predicted by JMatPro and revealed by DSC, SEM and TEM studies. Finally, it is found that the presence of Al_4Ca precipitates on the grain boundaries of Ca-added alloy prevents the growth of α(Al) by Zener pinning effect and results in the stability of microstructure during homogenization.

Key words: AlMg5 alloy; hot compression; homogenization; microstructure; particle stimulated nucleation; Zener pinning effect

1 Introduction

During the last decade, wrought Al−Mg alloys (5xxx series Al alloys) have attracted many attentions from the automotive industry [1,2]. This is mainly due to the good combination of mechanical properties, formability, weldability, and corrosion resistance [3−5]. Also, it is important to notice that the manufacturing cost of the 5xxx series is lower than that of heat- treatable 2xxx, 6xxx and 7xxx series that require additional thermal processes [6]. The mechanical properties of Al−Mg alloys depend mainly on their Mg content that results in solid solution strengthening [7].

Despite the beneficial effect of Mg content on the mechanical behavior of Al−Mg alloys, it is important to notice that, due to strong oxidation tendency of Mg, handling of Al alloys with high Mg content (ALMAG) is very difficult both in the molten and solid state [8−11]. Addition of a small amount of Be is reported to increase the oxidation

Corresponding author: Ashkan NOURI; Tel: +98-912-176-2635; Email: a-nouri@araku.ac.ir
DOI: 10.1016/S1003-6326(20)65236-0

resistance of molten Al−Mg. However, Be is toxic and causes lung cancer [12]. Therefore, an eco-friendly alternative is inevitable. Earlier studies show that the addition of Ca (in the form of Mg−Al_2Ca master alloy) improves the oxidation resistance of the Al−Mg alloys [13,14]. Kim's master alloy is produced by a simple addition of CaO into the molten Mg and Mg alloys. The details of Kim's method can be found elsewhere [13−15].

Although addition of Ca improves the oxidation resistance of ALMAG, it is of great importance to investigate its effects on the microstructure and deformation characteristics of these alloys. Investigations showed that hot compression behavior of the AlMg5 alloy made by Al_2Ca-containing master alloy is very different from that of the conventional AlMg5. Therefore, this study aimed to find out the origin of the above-mentioned difference.

2 Experimental

The chemical composition of the alloys and Al_2Ca-containing master alloy used in the study, as determined by inductively coupled plasma optical emission spectroscopy, is given in Table 1. AlMg5 alloy was produced by melting of Al (99.8% in purity) and Mg ingot (99.8% in purity) in a graphite crucible by an electric induction furnace. 0.4 wt.% of Al−5Ti−B grain refiner was added to the melt at 750 °C and the melt was then degassed by gas bubbling filtration (GBF) for 15 min with the argon gas flow rate of 8 L/min. Then, the melt (preheated to 200 °C) was poured into the metallic mold at 690 °C, as schematically shown in Fig. 1. The casting process of AlMg5Ca0.1 alloy was similar to that of AlMg5 alloy except for that Al_2Ca-containing master alloy was used instead of pure Mg. In this work, the AlMg5 alloy, AlMg5Ca0.1 alloys, and Al_2Ca-containing Mg master alloy are referred to AlMg, AlMgCa and master-alloy, respectively.

After complete solidification and then cooling to room temperature, cylindrical specimens with a diameter of 10 mm and height of 12 mm were machined from the castings (Fig. 1) and homogenized at 520 °C for 12 h followed by cooling to room temperature in air.

Mechanical behavior of the alloys was evaluated by a universal hot compression testing machine equipped with an electric resistance furnace. Since the thermal stability of the alloys was of great importance in this work, the hot compression tests were conducted at 400 and 500 °C which are quite high for aluminum alloys. The compression tests were carried out in the strain

Table 1 Chemical composition of alloys and master alloy used in this study (wt.%)

Alloy	Si	Fe	Cu	Mn	Mg	Ni	Zn	Ti	Zr	Ca	Al
AlMg5	0.035	0.065	0.004	0.009	4.71	0.011	0.006	0.0185	0.002	0.0039	Bal.
AlMg5Ca0.1	0.038	0.065	0.004	0.028	4.87	0.012	0.01	0.0198	0.002	0.0957	Bal.
Master-alloy	0.039	0.002	0.005	0.3	Bal.	0.002	0.056	−	−	1.03	5.94

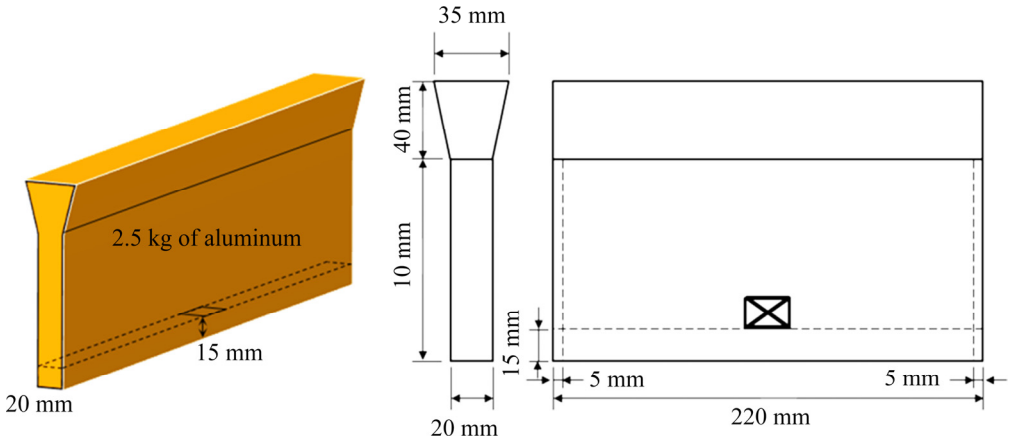

Fig. 1 Schematic of metallic mold used for casting and sampling position for hot compression test and metallurgical examinations

rate of 0.01 s^{-1}. Both sides of the hot compression test samples were lubricated by 0.25 mm-thick graphite film to minimize the friction between the sample and the tools. DSC (TA instrument SDT-Q600), optical microscopy (Nikon Eclipse MA200 with a polarizing filter, electrolytic etching by Barker's reagent), SEM along with energy-dispersive X-ray spectroscopy (EDX) (Bruker Quanta FEG 200), EBSD analysis (EDAX TSL OIM) and TEM (Tecnai G2, F30) were used for characterization of the alloys. JMatPro simulation software (Sente Software Ltd.) was also used for simulation of the solidification path of the alloys.

3 Results and discussion

Figure 2(a) shows the stress−strain curves obtained from the hot compression of the as-cast AlMg and AlMgCa alloys at 400 and 500 °C. It can be seen that at both temperatures, the flow behavior of both alloys is similar. The flow behavior of as-cast samples represents a rapid increase in stress up to a maximum value followed by a gradual decline to a stable plateau. This behavior resembles classic dynamic recrystallization (DRX) that includes work hardening up to peak stress followed by flow softening to steady-state deformation [16]. Generally, due to the high stacking fault energy, dynamic recovery (DRV) is the main softening mechanism during hot deformation of aluminum [17]. The addition of alloying elements such as Mg reduces the stacking fault energy of Al [18]. Therefore, the addition of Mg slows down the recovery processes and encourages the DRX. Several studies reported DRX during hot compression of Al−Mg alloys, especially in alloys with higher Mg content [19−21].

Figure 3 presents the optical microstructures of the examined alloys under the as-cast condition (Figs. 3(a) and 3(b)) and after homogenization at 520 °C for 12 h (Figs. 3(c) and 3(d)). Comparison of Figs. 3(a) and 3(b) (as-cast samples) reveals that the average grain size of as-cast AlMgCa alloy ((68±5) μm) is slightly smaller than that of as-cast AlMg alloy ((75±3) μm). This can be due to the role of Ca in enhancing the grain refinement effect of Al−Ti−B [22]. Therefore, the similar flow behavior of as-cast AlMg and AlMgCa alloys in Fig. 2(a) can be justified by their similar chemical composition and microstructure.

On the other hand, the stress−strain curves of the homogenized alloys (Fig. 2(b)) show different flow behaviors. So, at 400 °C, the stress−strain curve of the AlMgCa alloy shows the features of the classic DRX, i.e., the peak stress followed by a gradual decrease to the steady-state deformation. On the other hand, the AlMg alloy exhibits a slight gradual increase at the onset of the plastic deformation followed by a monotonic decrease at higher strains. Hence, no evidence of the steady-state deformation is seen up to the final strain of 0.7. Also, the peak stress of the homogenized AlMg alloy is higher and retarded at this temperature compared to that of the AlMgCa alloy. This relatively-broad peak stress and the gradual decline of stress will be discussed below according to the microstructure of the specimen. By increasing the temperature to 500 °C, the AlMg alloy shows steady-state flow stress after yielding, which indicates a dominant role of DRV.

In Al−Mg alloys, discontinuous DRX occurs during the hot deformation, where the strain-free

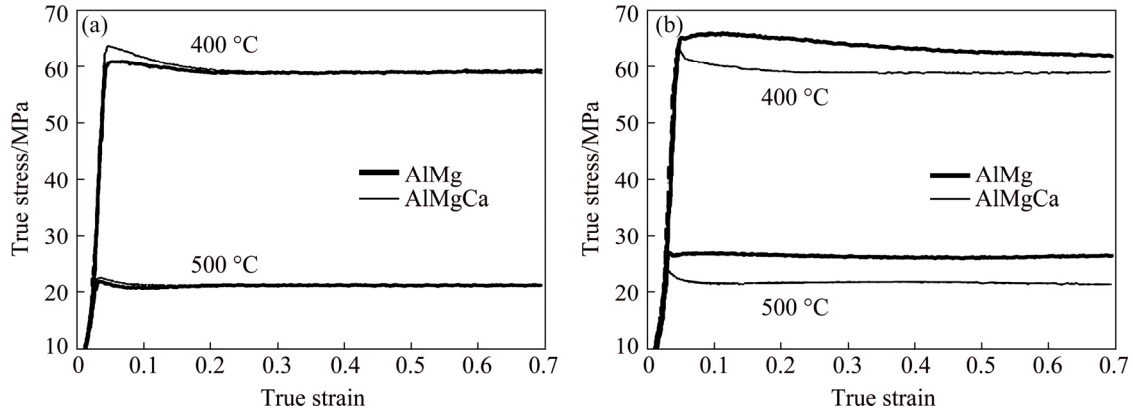

Fig. 2 True stress−strain curves of hot compression tests of AlMg and AlMgCa at 400 and 500 °C: (a) As-cast samples; (b) As-homogenized samples

grains nucleate and grow within the deformed microstructure [16]. The nuclei are usually initiated at the pre-existing grain boundaries and the equiaxed grains are formed in the microstructure during hot deformation. This is confirmed by EBSD orientation maps of the hot compressed (up to the strain of 0.7 at 500 °C) as-cast AlMg and AlMgCa alloys in Fig. 4. It can be seen that the pre-existing grains are decorated by necklaces of dynamically recrystallized grains. Therefore, the similar flow behavior of these samples during hot deformation (Fig. 2(a)) can be attributed to their similar microstructural evolutions.

In the as-cast samples, initiation and growth of new grains after a small critical strain oppose the work hardening. Thus, an acute drop can be seen after the peak stress. There is the same mechanism along with an acute drop after the peak stress during the hot deformation of the fine-grained (Fig. 3(d)) homogenized AlMgCa alloy. Comparison of the microstructure of the as-cast and homogenized AlMgCa samples (Figs. 3(b) and 3(d)) shows that

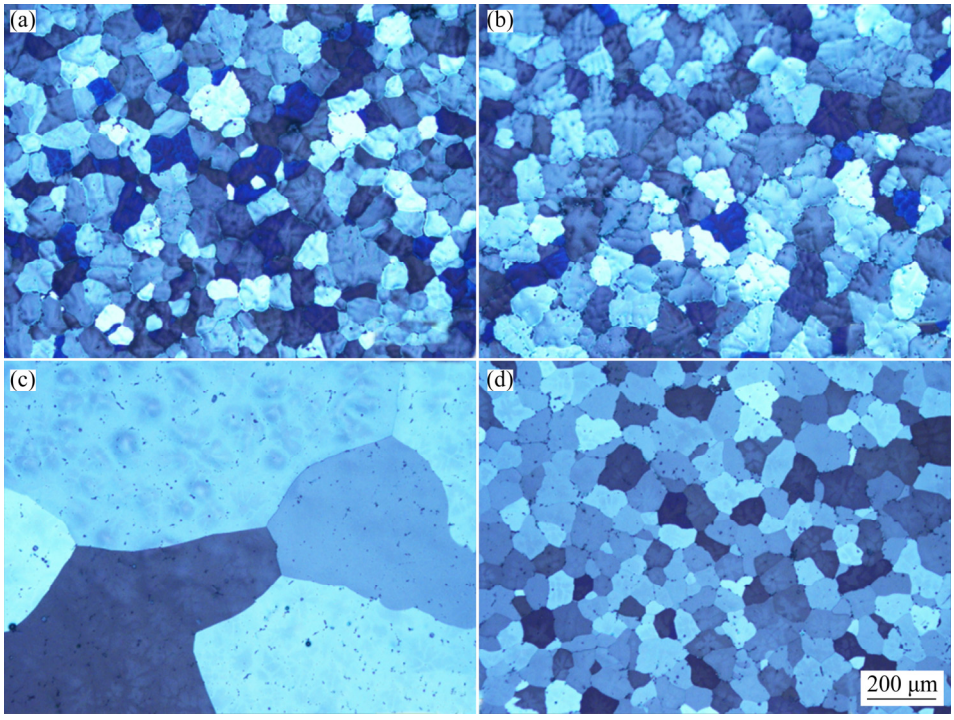

Fig. 3 As-cast microstructures of AlMg (a) and AlMgCa (b) alloys and homogenized microstructures of AlMg (c) and AlMgCa (d) alloys (Images are obtained by a polarized optical microscope)

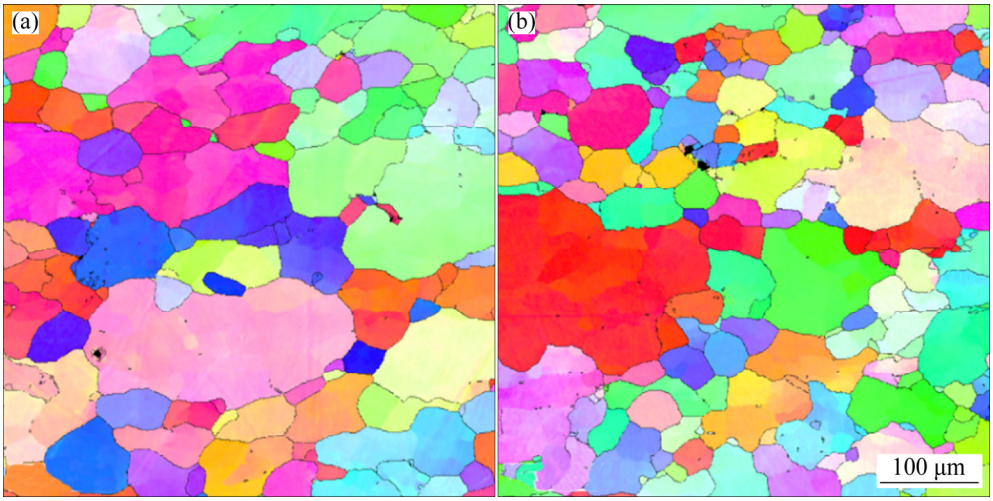

Fig. 4 EBSD micrographs of as-cast AlMg (a) and AlMgCa (b) alloys compressed (without homogenization) to strain of 0.7 at 500 °C

no significant growth occurs during the homogenization of AlMgCa alloy. This implies the presence of sufficient number of nucleation sites during the hot deformation of AlMgCa alloy.

On the other hand, the comparison of Figs. 3(a) and 3(c) reveals that unlike the AlMgCa alloy, a drastic grain growth occurs in AlMg alloy during homogenization at 520 °C for 12 h. Thus, the grain boundary area decreases. Since the grain boundaries act as nucleation sites, the DRX occurs with a relatively long delay due to the low fraction of grain boundaries. This provides enough time for DRV in the homogenized AlMg alloy in which the effects of softening are more pronounced in comparison to the specimens with finer grain sizes, i.e., the as-cast alloys (AlMg and AlMgCa) and the homogenized AlMgCa alloy.

The initial coarse grains of the homogenized AlMg alloy (Fig. 3(c)) explain the slow drop of stress on its flow curve (Fig. 2(b)). Also, the cases with fine initial grains (i.e., as-cast AlMg and AlMgCa alloys and the homogenized AlMgCa alloy) show lower steady-state stress values than the homogenized AlMg alloy with coarse grains. This indicates that the steady-state microstructure is not yet reached for the coarse grain samples.

It is reported [16,23] that the steady-state flow stress is controlled by the Zener−Hollomon parameter (as a function of strain rate and temperature) and is independent on the initial grain size. Therefore, the rest of this study is focused on the formation of the second phase particles during the solidification of the AlMgCa alloy and the effects of these particles on the change of the microstructure during homogenization and hot compression.

The second phase particles were investigated by DSC and JMatPro package that provides information about the solidification path of the alloys and the constituents of the microstructure. The simulation of the solidification path of the examined alloys was conducted in the Scheil−Gulliver regime for predicting a non-equilibrium solidification condition [24]. The results of simulation by JMatPro and the results of DSC analysis are presented in Figs. 5 and 6, respectively.

From Fig. 5(a), solidification of the AlMg alloy starts with the formation of α(Al) at 638 °C, followed by the formation of Al_3Fe at 579 °C, Mg_2Si at 517 °C and β-Al_3Mg_2 (also called Mg_5Al_8) at 449 °C. For AlMgCa alloy (Fig. 5(b)), α(Al), Al_3Fe, Mg_2Si and Al_3Mg_2 start to form at 637, 579, 522 and 447 °C, respectively. Although comparison of Figs. 5(a) and 5(b) shows that the addition of 0.1 wt.% Ca does not significantly affect the formation temperature of the main constituents, Fig. 5(b) shows that the addition of 0.1 wt.% Ca results in the formation of a new phase (Al_4Ca) at 483 °C.

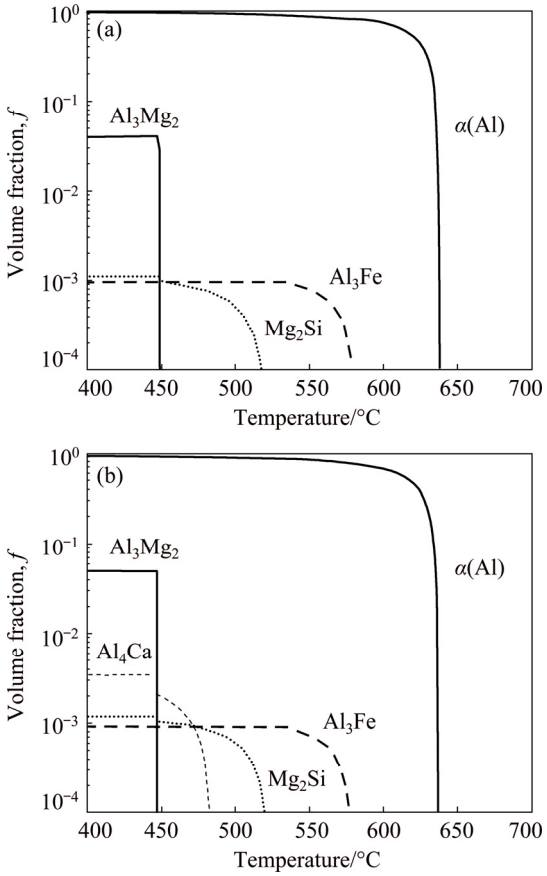

Fig. 5 Simulation of solidification path of AlMg (a) and AlMgCa (b) with JMatPro

Figure 6 shows the DSC curves of the examined alloys and their corresponding first derivatives. The DSC analysis was carried out with heating and cooling rate of 20 °C/min, close to the Scheil−Gulliver regime. In Fig. 6(a), paired peaks 1−1′, 2−2′ and 3−3′ belong to α(Al), Al_3Fe and Mg_2Si, respectively. From the result of DSC analysis of AlMgCa alloy in Fig. 6(b), the paired peaks 1−1′, 2−2′, 3−3′ belong to α(Al), Al_3Fe and Mg_2Si, respectively, and 4−4′ pair belongs to Al_4Ca phase. Therefore, the comparison of Figs. 6(a) and 5(a) as well as Figs. 6(b) and 5(b) confirms that the obtained results by JMatPro are reliable. The DSC analysis of AlMgCa alloy in Fig. 6(b) shows that Al_4Ca phase starts to form at 526 °C. On the

other hand, according to binary Al−Mg phase diagram [25], the equilibrium solidus temperature is about 593 °C for Al−4.7%Mg alloy (the same magnesium content with the used alloy). This means that the initial formation temperature of the Al_4Ca phase is about 70 °C below the solidus temperature of the AlMgCa alloy. Furthermore, Fig. 5(b) shows that 92% of AlMgCa alloy is solidified before the formation of Al_4Ca phase. Therefore, it is reasonable to conclude that Al_4Ca particles essentially precipitate at the grain boundaries of α(Al). Other researchers [26] have also reported that Ca segregates to the grain boundaries.

The DSC analysis and the results of simulation by JMatPro show that addition of Ca results in the formation of the new phase, Al_4Ca, which distributes in AlMgCa alloy. This finding was further investigated by SEM and TEM. The SEM/BSE images of Fig. 7 show the as-cast

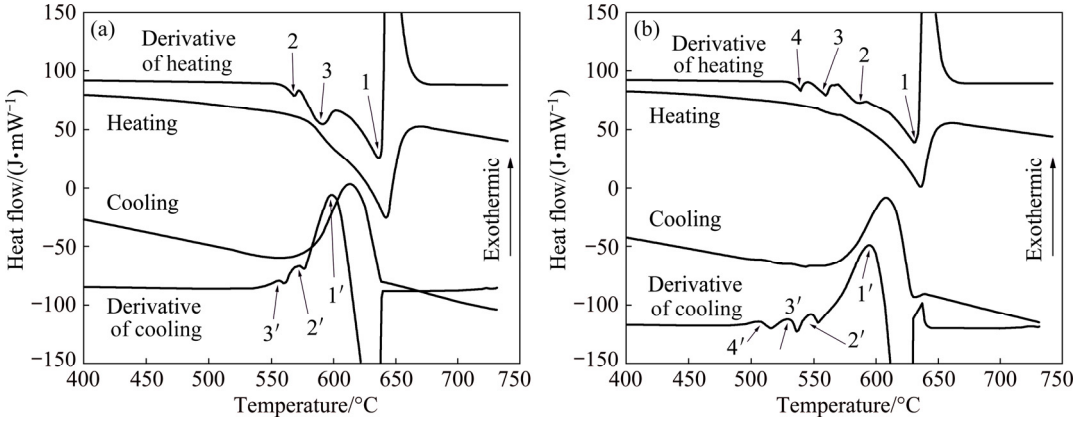

Fig. 6 Heating and cooling DSC curves and corresponding first derivatives of AlMg (a) and AlMgCa (b) alloys (Rate of heating and cooling is 20 °C/min)

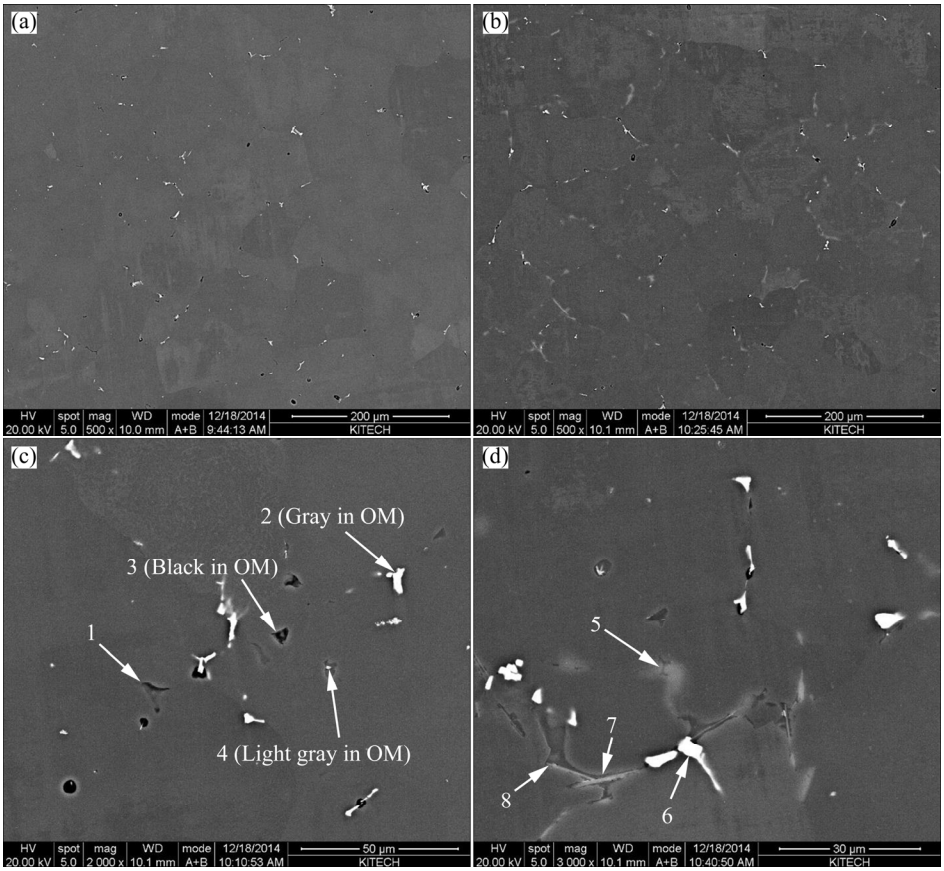

Fig. 7 SEM/BSE images showing as-cast microstructures of AlMg alloy (a, c) and AlMgCa (b, d) alloy along with selected points for EDX analyses

microstructures of the alloys. The chemical composition of the selected points is given in Table 2. From Fig. 7, both alloys have a similar as-cast microstructure that contains grains of primary aluminum, Al_3Fe, and Mg_2Si particles. Also, Fig. 7(d) shows that there are some Ca-containing particles within the microstructure of the AlMgCa alloy.

Table 2 EDS analysis results of selected points in Fig. 7

No.	Content/at.%					Remarks
	Al	Mg	Fe	Si	Ca	
1	94.53	5.47	−	−	−	Matrix
2	82.1	4.95	12.95	−	−	Al_3Fe
3	55.52	23.79	−	16.18	−	Mg_2Si
4	71.38	24.91	−	1.22	−	Al_3Mg_2
5	71.34	21.93	−	−	6.73	Mg−Ca
6	80.26	4.55	15.19	−	−	Al_3Fe
7	59.37	20.89	−	10.7	9.03	Mg−Si−Ca
8	77.16	22.46	−	−	0.38	Al_3Mg_2

Figure 8 shows the SEM/BSE images of microstructures of the homogenized samples. The EDS analysis result of the selected points is presented in Table 3. Comparison of the distribution of the particles in Figs. 8(a) and 8(b) (located in grain boundaries) reveals that the grains of the homogenized AlMg alloy are considerably larger than those of AlMgCa alloy. This is despite the fact that these alloys have similar as-cast microstructures. However, the microstructure of the homogenized AlMgCa alloy in Fig. 8(b) is comparable to its as-cast condition in Fig. 7(b). Comparison of Figs. 8(a) and 7(a) shows that homogenization of the AlMg alloy results in remarkable grain growth in this alloy.

Figures 9(a) and 9(b) show that the size of second phase particles (white particles) is relatively large. It has been reported that during hot deformation, the coarse second phase particles may lead to grain refinement by particle stimulated nucleation (PSN) mechanism [16,23,27]. Also, the concentration of plastic flow in the vicinity of hard

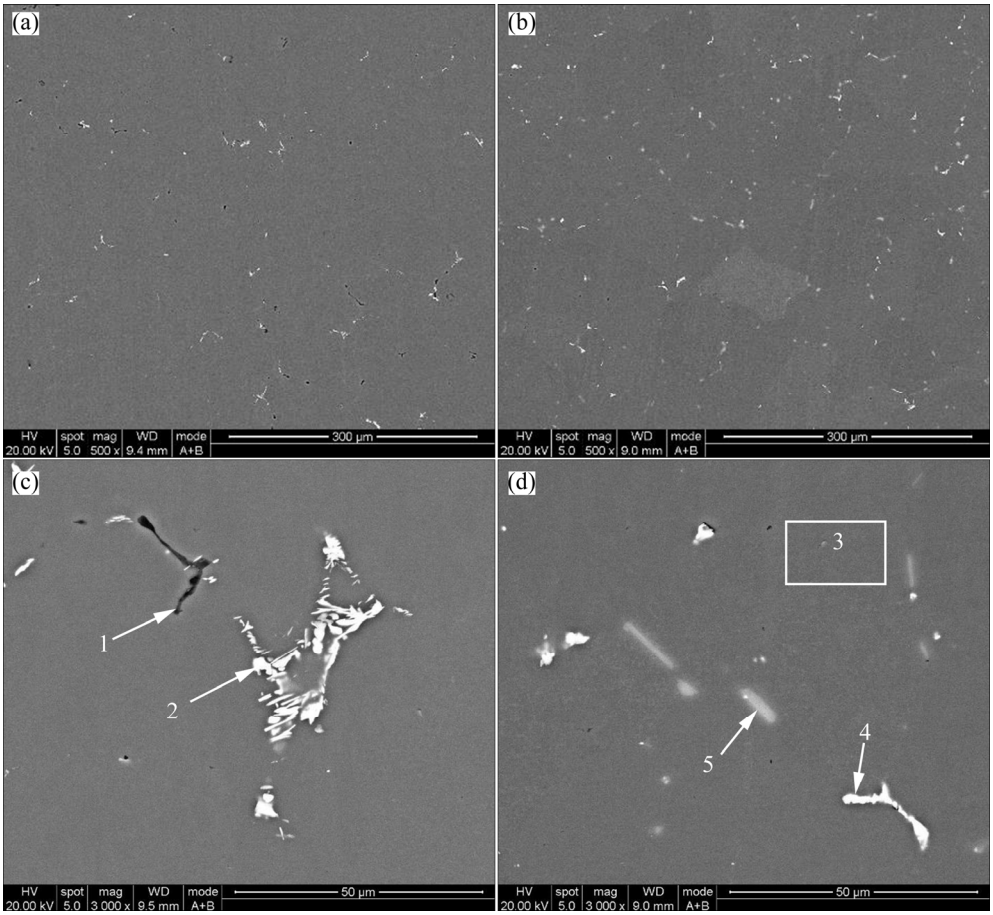

Fig. 8 SEM/BSE images showing microstructure of AlMg alloy (a, c) and AlMgCa alloy (b, d) after homogenization at 520 °C for 12 h with selected points for EDX analyses

Table 3 EDS analysis results of selected points in Fig. 8

No.	Content/at.%					Remarks
	Al	Mg	Fe	Si	Ca	
1	91.4	4.75	3.85	−	−	Al_3Fe
2	87.85	7.11	−	5.04	−	Mg_2Si
3	93.36	6.64	−	−	−	Matrix
4	81.56	2.62	10.56	−	5.25	Al_3Fe(Ca)
5	64.46	12.54	−	12.73	10.27	Mg−Si−Ca

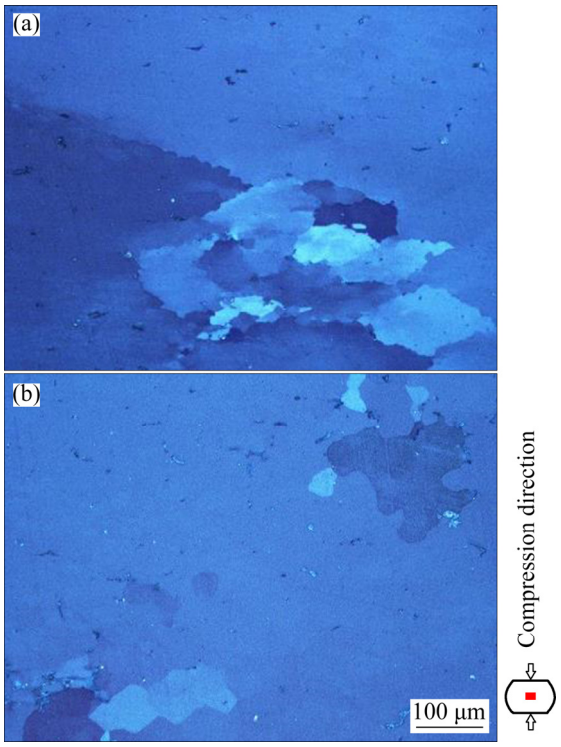

Fig. 9 Optical micrographs of homogenized AlMg alloy after hot compression to strain of 0.7 with strain rate of 0.01 s^{-1} at 400 °C (a) and 500 °C (b)

particles leads to a heterogeneous pile-up of dislocations around the particles and appearance of a deformation zone with large misorientation gradient [16,27]. These high energy regions provide suitable sites for nucleation of new recrystallized grains.

Figures 7 and 8 show that both as-cast and homogenized microstructures of both examined alloys contain a large number of coarse second phase particles. In the case of homogenized AlMg alloy, which has coarser grains, due to the low fraction of the grain boundaries and consequent low nucleation rate, the PSN mechanism plays a more significant role in the formation of new grains than that in the homogenized AlMgCa alloy that has finer microstructure. Figure 9 shows the occurrence of PSN in homogenized AlMg alloy in which the fine equiaxed grains locally form in the vicinity of a particle and the rest of the microstructure is free of recrystallized grains.

Figure 10 shows the microstructure and the SEM/EDS obtained from the homogenized AlMgCa alloy. The EDS map in Fig. 10(b) reveals that the Ca-containing particles (the light particles in Fig. 8(d)) are precipitated on the grain boundaries of the primary aluminum phase. Also, the EDS line scan in Fig. 10(c) shows the variation of Ca along the analysis line in which the bright particles contain a considerable amount of Ca in their chemical composition. These observations confirm the previous conclusion about the precipitation of Ca-containing compounds (probably Al_4Ca) on the grain boundaries of α(Al).

The TEM micrograph of the homogenized AlMgCa sample and the chemical analysis results of the selected points are shown in Fig. 11. The solid and dotted arrows indicate the grain boundary of α(Al) and the Ca-containing particles, respectively. The EDS analysis of the points 1 and 2 shows that they contain a considerable amount of Ca in their chemical composition. It can be seen that these particles are precipitated in the boundaries of primary aluminum phases. The selected area diffraction pattern of Particle 1 (in Fig. 11(a)) is presented in Fig. 11(b). It is seen that no preferential orientation relationship exists between the tetragonal Ca-bearing compound (Al_4Ca) and aluminum matrix. The Al_4Ca particles can be considered as effective Zener-pinning agents that prevent grain growth of α(Al) grains during homogenization. This effect can be clearly seen during the homogenization of as-cast alloys with and without Ca. Figures 3(c) and 3(d) represent the microstructures of the as-cast alloys after homogenization at 520 °C for 12 h. In AlMgCa alloy (Fig. 3(d)) due to the presence of fine Al_4Ca particles and Zener pinning effect, the microstructure is stable and homogenization does not change the grain size significantly. However, in AlMg alloy, the Zener drag doesn't play any important role in the grain growth. So, the average grain sizes in the homogenized alloys with and without Ca are significantly different. Therefore, it can be concluded that the combined effects of PSN and Zener-pinning result in the formation of fine microstructure in AlMgCa alloy.

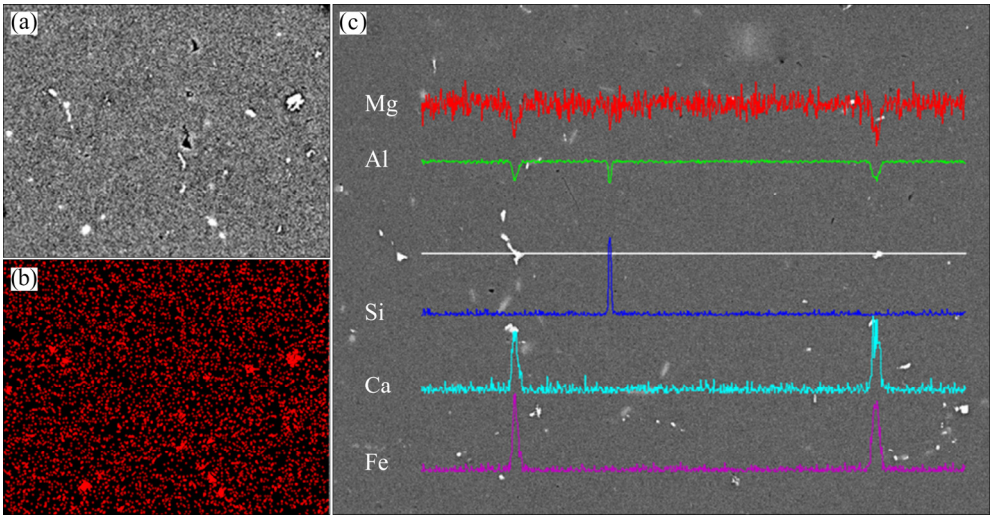

Fig. 10 SEM image (a), corresponding EDS map (b) and EDS line scan (c) indicating presence of Ca-containing particles within microstructure of homogenized AlMgCa alloy

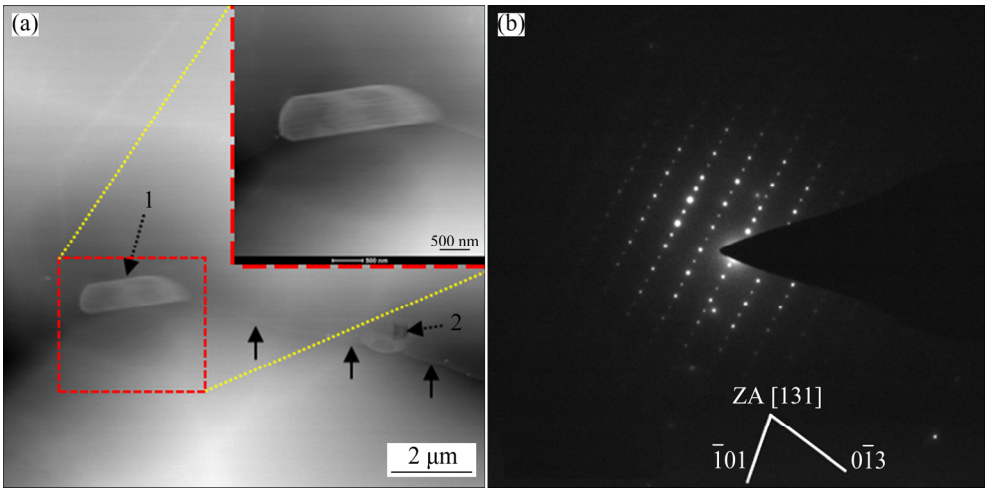

Fig. 11 TEM image showing Al_4Ca particles on grain boundary of α(Al) (a) and selected area diffraction pattern (b) of Particle 1 in (a)

4 Conclusions

(1) Addition of a minor amount of Ca does not alter the as-cast microstructure of the AlMg5 alloy, so that the both Ca-free and Ca-added samples show similar microstructures.

(2) During the hot compression at 400 and 500 °C, both Ca-free and Ca-added AlMg5 samples show similar stress−strain behavior that can be explained by their similar initial microstructure.

(3) Homogenization at 520 °C for 12 h results in a drastic grain growth in Ca-free AlMg5 alloy. However, the precipitation of Al_4Ca particles on the grain boundaries of primary aluminum phase of Ca-added AlMg5 alloy stabilizes the microstructure of this alloy and prevents grain growth during homogenization.

(4) The coarse initial microstructure of homogenized Ca-free AlMg5 alloy clearly postpones the DRX during the hot deformation due to the fewer nucleation sites which provide enough time for DRV. This explains the flow behavior of the homogenized Ca-free AlMg5 alloy in hot compression, i.e., a relatively broad peak stress followed by a gradual softening.

Acknowledgments

This work was supported by the research project on aluminum alloys (Grant No. PJE18070

of Korea Institute of Industrial Technology), which is funded by Ministry of Trade, Industry and Energy, Korea.

References

[1] MA Ming-tu, ZHANG Jun-ping, ZHOU Jia, LU Hong-zhou. Property requirements and research progress of aluminum alloy sheets for automotive closure [J]. Materials Science Forum, 2018, 913: 18−29.

[2] ZHOU J, ZHANG J P, YAN H L, MA M T. Research on the deformation behavior of aluminum alloy sheets under various temperatures [C]//Advanced High Strength Steel and Press Hardening: Proceedings of the 3rd International Conference on Advanced High Strength Steel and Press Hardening (ICHSU2016). World Scientific, 2017: 59−65.

[3] LONG R S, BOETTCHER E, CRAWFORD D. Current and future uses of aluminum in the automotive industry [J]. JOM, 2017, 69: 2635−2639.

[4] LEO P, RENNA G, CASALINO G, OLABI A G. Effect of power distribution on the weld quality during hybrid laser welding of an Al−Mg alloy [J]. Optics & Laser Technology, 2015, 73: 118−126.

[5] ZHANG Rui-feng, QIU Yao, QI Yuan-shen, BIRBILIS N. A closer inspection of a grain boundary immune to intergranular corrosion in a sensitised Al−Mg alloy [J]. Corrosion Science, 2018, 133: 1−5.

[6] SANDERS R E, HOLLINSHEAD P, SIMIELLI E A. Industrial development of non-heat treatable aluminum alloys [J]. Materials Forum, 2004, 28: 53−64.

[7] LEE Byeong-Hyeon, KIM Sung-Hoon, PARK Jun-Hyoung, KIM Hyung-Wook, LEE Jae-Chul. Role of Mg in simultaneously improving the strength and ductility of Al−Mg alloys [J]. Materials Science and Engineering A, 2016, 657: 115−122.

[8] KIM S K, OH G Y, YOON Y O. Oxidation resistances of Al_2Ca added Al-5 Mg alloy [C]//AIP Conference Proceedings. United States: American Institute of Physics, 2012.

[9] YOON Young-ok, HA Seong-ho, YEOM Gil-yong, LIM Hyun-kyu, KIM Shae K. Oxidation behavior of Al2Ca added Al−5Mg alloy in the liquid state [J]. Light Metals, 2016: 323−326.

[10] EISAABADI B G, TIRYAKIOĞLU M, YEOM G Y, NETTO N, BEYGI R, ZAREZADEH M M, KIM Shae K. The effect of solution treatment time on the tensile deformation characteristics of naturally-aged A383 alloy die castings [J]. Materials Science and Engineering A, 2018, 731: 80−84.

[11] EISAABADI B G, YEOM G Y, TIRYAKIOĞLU M, NETTO N, BEYGI R, ZAREZADEH M M, KIM Shae K. The effect of solution treatment time on the microstructure and ductility of naturally-aged A383 alloy die castings [J]. Materials Science and Engineering A, 2018, 722: 1−7.

[12] LEE Jin Kyu, KIM Shae K. Development of novel environment-friendly magnesium alloys [J]. Advanced Materials Research, 2008, 47: 940−943.

[13] LEE Taeg-woo, PARK Hyun-woong, LIM Hyunkyu, KIM Shae K, LIM Sung-hwan. Microstructural characterization of oxide layers in CaO added AZ31 Mg alloy [J]. Journal of Alloys and Compounds, 2017, 714: 397−408.

[14] JUNG In-ho, LEE Jin-kyu, KIM Shae K. Mg−Ca alloys produced by reduction of CaO: Understanding of ECO-Mg alloy production [J]. Metallurgical and Materials Transactions B, 2017, 48: 1073−1078.

[15] KIM S K, SEO J H. Magnesium-based alloy with superior fluidity and hot tearing resistance and manufacturing method thereof: US 8734564 B2 [P]. 2014−05−27.

[16] HUMPHREYS F J, HATHERLY M. Recrystallization and related annealing phenomena [M]. Elsevier, 2012.

[17] WU Bin, LI Miao-quan, MA Dong-wei. The flow behavior and constitutive equations in isothermal compression of 7050 aluminum alloy [J]. Materials Science and Engineering A, 2012, 542: 79−87.

[18] QI Yue, MISHRA R K. Ab initio study of the effect of solute atoms on the stacking fault energy in aluminum [J]. Physical Review B, 2007, 75(22): 224105.

[19] SHEPPARD T, TUTCHER M G. Development of duplex deformation substructure during extrusion of a commercial Al−5Mg−0.8Mn Alloy [J]. Metal Science, 1980, 14: 579−590.

[20] RAGHUNATHAN N, ZAIDI M A, SHEPPARD T. Recrystallization kinetics of Al−Mg alloys AA 5056 and AA 5083 after hot deformation [J]. Materials Science and Technology, 1986, 2: 938−945.

[21] HUANG Ke, LOGÉ R E. The flow stress evolution and grain refinement mechanisms during hot deformation of Al−Mg alloy [J]. Procedia Engineering, 2017, 207: 25−30.

[22] KUMARI S S S, PILLAI R M, PAI B C. Role of calcium in aluminium based alloys and composites [J]. International Materials Reviews, 2005, 50(4): 216−238.

[23] HUANG Ke, LOGÉ R E. A review of dynamic recrystallization phenomena in metallic materials [J]. Materials and Design, 2016, 111: 548−574.

[24] SPIERINGS A B, DAWSON K, HEELING T, UGGOWITZER P J, SCHÄUBLIN R, PALM F, WEGENER K. Microstructural features of Sc- and Zr-modified Al−Mg alloys processed by selective laser melting [J]. Materials and Design, 2017, 115: 52−63.

[25] MEZBAHUL-ISLAM M, MOSTAFA A O, MEDRAJ M. Essential magnesium alloys binary phase diagrams and their thermochemical data [J]. Journal of Materials, 2014, 2014: 1−32.

[26] HORIKAWA K, KURAMOTO S, KANNO M. Intergranular fracture caused by trace impurities in an Al−5.5 mol% Mg alloy [J]. Acta Materialia, 2001, 49: 3981−3989.

[27] WANG Xiao-feng, GUO Ming-xing, ZHANG Yan, XING Hui, LI Yong, LUO Jin-ru, ZHANG Ji-shan, ZHUANG Lin-zhong. The dependence of microstructure, texture evolution and mechanical properties of Al−Mg−Si−Cu alloy sheet on final cold rolling deformation [J]. Journal of Alloys and Compounds, 2016, 657: 906−916.

Ca 对 AlMg5 合金均匀化过程中热压缩行为和微观结构稳定性的影响

Bong Huang KIM[1,2], Majid SEYED SALEHI[3], Ashkan NOURI[4], Mohammad Sadegh MOHEBI[5], Seong Ho HA[1], Young Ok YOON[1], Hyun Kyu LIM[1], Shae K. KIM[1], B. Ghasem EISAABADI[4]

1. Korea Institute of Industrial Technology, 156 Gaetbeol-ro, Yeonsu-gu, Incheon 21999, Korea;
2. Department of Materials Science & Engineering, Yonsei University, 262 Seongsan-ro, Seodaemun-gu, Seoul 120-749, Korea;
3. Faculty of Materials Science and Engineering, K. N. Toosi University of Technology, Tehran, Iran;
4. Department of Materials Science and Engineering, Faculty of Engineering, Arak University, Arak 38138-5-3945, Iran;
5. Department of Mechanical Engineering, Qom University of Technology, Qom, Iran

摘　要：研究微量 Ca 添加对 AlMg5 热变形过程中微观结构稳定性和动态回复行为的影响。研究手段包括扫描电子显微术(SEM)、差示扫描量热法(DSC)、电子背散射衍射(EBSD)分析和透射电子显微术(TEM)。利用 JMatPro 程序包对合金的凝固路径进行模拟。结果表明，Ca 的加入对铸态试样的显微组织和热压缩行为没有影响，但能阻止均匀化过程中晶粒的急剧长大。在热压缩过程中，无 Ca 合金中的粗晶粒促进合金的动态回复，减缓动态再结晶，其再结晶晶粒的主要形核机制是粒子激发形核。另一方面，热压缩含 Ca 合金的显微组织受到 Al_4Ca 金属间化合物的显著影响。通过 JMatPro 预测，并通过 DSC、SEM 和 TEM 揭示 Al_4Ca 相的形成。最后，在含 Ca 合金的晶界处发现 Al_4Ca 析出相通过 Zener 钉扎效应阻碍 α(Al)相的增长，提高均匀化过程中微观结构的稳定性。

关键词：AlMg5 合金；热压缩；均匀化；显微组织；粒子激发形核；Zener 钉扎效应

(Edited by Bing YANG)